

Optimal Aeroacoustic Shape Design Using a Discrete Adjoint Approach

Markus P. Rumpfkeil and David W. Zingg

University of Toronto Institute for Aerospace Studies, 4925 Dufferin Street, Toronto, ON, M3H 5T6, Canada

Email: *markus@oddjob.utias.utoronto.ca*

ABSTRACT

In this paper, shape optimization is used to minimize aerodynamic noise in an unsteady trailing-edge flow. First, a generic time-dependent optimal design problem is introduced and the derivation of the discrete adjoint equations in a general approach is outlined. The presented framework is then applied to a time-dependent laminar flow past an acoustically compact airfoil. The results show a significant reduction of up to 95 percent in the total radiated acoustic power with reasonable computational cost using twelve shape design variables.

1 INTRODUCTION AND MOTIVATION

The majority of work in aerodynamic shape optimization in the past has focused on the design of aerospace vehicles in a steady flow environment [1, 2, 3, 4]. Researchers have applied these advanced design algorithms, particularly the adjoint method, to numerous problems, ranging from the design of two-dimensional airfoils to full aircraft configurations to decrease drag, increase lift, and so on. These problems have been approached using many different numerical schemes on both structured and unstructured grids.

The application of numerical optimization to airframe-generated noise, however, has not received as much attention, but with the significant quieting of modern engines, airframe noise now competes with engine noise [5]. Thus airframe-generated noise is an important component of the total noise radiated from commercial aircraft, especially during aircraft approach and landing, when engines operate at reduced thrust, and airframe components (such as high-lift devices) are in the deployed state [6]. Future Federal Aviation Administration noise regulations, the projected growth in air travel and the increase in population density near airports will require future civil aircraft to be substan-

tially quieter than current ones. Consequently, the attempt to understand and reduce airframe noise has become an important research topic [7].

Optimal control techniques for unsteady flows are needed in order to be able to reduce airframe-generated noise. This paper presents a general framework to calculate the gradient in a nonlinear unsteady flow environment via the discrete adjoint method. The presented framework is then applied to an aerodynamic noise reduction problem involving unsteady laminar trailing-edge flow similar to the one presented by Marsden *et al.* [8].

2 FORMULATION OF THE DISCRETE TIME-DEPENDENT OPTIMAL CONTROL PROBLEM

In the following we assume that we control an unsteady flow in the time interval $[0, T]$ with an initial flow solution Q^0 at $t = 0$. In this section we use the implicit Euler time marching method to discretize the governing equations in time. This is not a restriction, since it is straightforward to modify the equations to use any other time marching method (e.g. see Rumpfkeil and Zingg [9] for the derivation with the second-order backwards difference (BDF2) time-marching method as used to obtain the results presented in this paper).

We introduce a cost function

$$J = \sum_{n=1}^N I^n(Q^n, Y), \quad (1)$$

where the function $I^n = I^n(Q^n, Y)$ depends on the time-dependent flow solution Q^n and design variables Y for $n = 1, \dots, N$. N can be calculated from the relation $T = N\Delta t$, where Δt is the chosen time discretization step. We then assume that $R = R(Q^n, Y)$ contains the

spatially discretized convective and viscous fluxes as well as the boundary conditions and that

$$R^{*n}(Q^n, Q^{n-1}, Y) := \frac{Q^n - Q^{n-1}}{\Delta t} + R(Q^n, Y) = 0 \quad (2)$$

defines implicitly the time-dependent flow solution Q^n for $n = 1, \dots, N$. We use an inexact-Newton strategy to drive $R^{*n} = R^{*n}(Q^n, Q^{n-1}, Y)$ to zero [10, 11]. It does not matter how one solves equation (2) as long as $R^{*n} = 0$ for all n , since this is the requirement for the following derivation.

The task of minimizing the cost function J subject to $R^{*n} = 0$ for all n can now be written as an unconstrained optimization problem of minimizing the Lagrangian function

$$\mathcal{L} = \sum_{n=1}^N [I^n(Q^n, Y) + (\psi^n)^T R^{*n}(Q^n, Q^{n-1}, Y)] \quad (3)$$

with respect to Q^0, \dots, Q^N and ψ^1, \dots, ψ^N , where ψ^1, \dots, ψ^N are the N vectors of Lagrange multipliers. A necessary condition for an extremal is that the gradient of \mathcal{L} with respect to Q^0, \dots, Q^N and ψ^1, \dots, ψ^N should vanish. Since we start with Q^0 and calculate the states Q^1, \dots, Q^N using the constraints given by equation (2), we ensure that $\nabla_{\psi^n} \mathcal{L} = 0$ for $n = 1, \dots, N$ automatically.

The Lagrange multipliers ψ^n must now be chosen such that $\nabla_{Q^n} \mathcal{L} = 0$ for $n = 1, \dots, N$, which leads to

$$0 = \nabla_{Q^n} I^n + (\psi^n)^T \nabla_{Q^n} R^{*n} + (\psi^{n+1})^T \nabla_{Q^n} R^{*n+1} \quad (4)$$

for $n = 1, \dots, N-1$

$$0 = \nabla_{Q^N} I^N + (\psi^N)^T \nabla_{Q^N} R^{*N}. \quad (5)$$

This can be written equivalently as

$$\psi^N = -((\nabla_{Q^N} R^{*N})^T)^{-1} (\nabla_{Q^N} I^N)^T \quad (6)$$

$$\psi^n = -((\nabla_{Q^n} R^{*n})^T)^{-1} [(\nabla_{Q^n} I^n)^T + (\nabla_{Q^n} R^{*n+1})^T \psi^{n+1}] \quad (7)$$

for $n = N-1, \dots, 1$.

Since Q^1, \dots, Q^N have been calculated from the current guess of Y , the Lagrange multipliers ψ^n can be calculated recursively backwards from the terminal boundary condition (6) using (7). The system of equations (6) and (7) is known as the system of adjoint equations for the model (2), or as the adjoint model. In this context, the Lagrange multipliers are also known as the adjoint variables.

Finally, one can evaluate the gradient of J with respect to the design variables Y , which can then be

used in a gradient-based optimization algorithm such as BFGS [12, 13, 14, 15] to find the optimum:

$$\frac{\partial J}{\partial Y} = \frac{\partial \mathcal{L}}{\partial Y} = \sum_{n=1}^N [\nabla_Y I^n(Q^n, Y) + (\psi^n)^T \nabla_Y R(Q^n, Y)]. \quad (8)$$

In summary, the gradient is determined by the solution of the adjoint equations in reverse time from the terminal boundary condition and the partial derivatives of the flow residual and objective function with respect to the design variables (while Q^n is held constant). One can also see that the computational costs of unsteady optimization problems are directly proportional to the desired number of time steps and (almost) independent of the number of design variables.

3 OUTLINE OF THE AERODYNAMIC NOISE REDUCTION PROBLEM

We now present an unsteady noise reduction problem which applies the above framework in practice. The airfoil geometry shown in Figure 1 is a shortened version of the airfoil used in the experiments of Blake [16] and is very similar to the one used by Marsden *et al.* [8] in their noise minimization using a surrogate management framework. The airfoil chord is 10 times its thickness, the free stream Mach number is $M_\infty = 0.2$ with a Reynolds number of $Re = 10,000$, and the angle of attack is 0° .

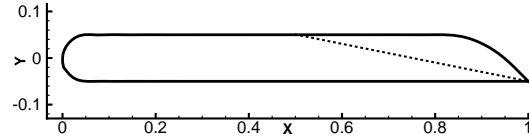


Figure 1: Blake airfoil used in unsteady laminar flow problem with the thickness constraint line (dotted). The upper right half of the surface is allowed to deform.

For unsteady laminar flow past an airfoil at low Mach number, the acoustic wavelength associated with the vortex shedding is typically long relative to the airfoil chord [8]. The noise generation from such an acoustically compact airfoil can be expressed using Curle's extension to the Lighthill theory [17] and a cost function directly proportional to the total radiated acoustic power can be derived [18]:

$$J = \overline{\left(\frac{\partial}{\partial t} \int_S n_j p_{1j}(y, t) ds \right)^2} + \overline{\left(\frac{\partial}{\partial t} \int_S n_j p_{2j}(y, t) ds \right)^2}, \quad (9)$$

where $p_{ij} = p\delta_{ij} - \tau_{ij}$ is the compressive stress tensor, composed of pressure and viscous stress, n_j are

the normalized components of the outward normal to the airfoil surface \mathcal{S} , and y is the airfoil surface or source field position vector. The overbar denotes time-averaging, and repeated indices follow the usual Einstein summation convention. The radiation in this case is of dipole type, caused by the fluctuating lift and drag forces; the reader is referred to Wang *et al.* [19] for more details on airfoil self-noise due to vortex shedding.

The geometry of the airfoil is described with cubic B-spline curves [4], which means that some of the y -coordinates of the B-spline control points in the upper right half of the airfoil can easily be used as shape design variables. Since the cost of our adjoint approach is independent of the number of design variables, we decided to use considerably more shape design variables than the five that Marsden *et al.* [8] could afford in their study using a surrogate management framework. We use twelve shape design variables in this research, thus giving the airfoil more freedom in the design space to take the most beneficial shape as given by the BFGS optimizer [20, 21]. However, we impose thickness constraints to ensure that the airfoil has a certain minimum thickness via a quadratic penalty method. We apply the same minimum thickness as imposed by Marsden *et al.*, which is given by a straight line connecting the left edge of the deformation region and the trailing edge, as shown in Figure 1.

In order to solve the underlying two-dimensional unsteady Navier-Stokes equations, we use a C-mesh with 248×95 nodes, the second-order backwards difference (BDF2) time-marching method and our single-block structured solver, PROBE [11], which is a Newton-GMRES solver loosely based on ARC2D [22]. We actually only solve the thin-layer Navier-Stokes equations in non-dimensional form with the following scaling parameters: the free stream density ρ_∞ , the airfoil chord c as length scale, the free stream speed of sound a_∞ as velocity scale, and c/a_∞ as time scale. However, our Reynolds number of 10,000 is still based on the free stream velocity u_∞ . Marsden *et al.* used a very similar scaling to present their results, although they used u_∞ as the velocity scale. In order to convert the objective function value from our scaling to Marsden’s scaling we have to divide it by $(M_\infty)^6$ and we have to multiply our non-dimensionalized time by M_∞ to be able to compare it to Marsden’s non-dimensionalized time. For the remainder of this paper we will report all our results with Marsden’s scaling to make comparisons easier.

To solve the linear systems in the adjoint equations the preconditioned Bi-CGSTAB algorithm [23] is used

with an absolute convergence tolerance of 10^{-12} . We found that Bi-CGSTAB is about fifty percent faster than the preconditioned generalized minimum residual (GMRES) method [24], which we use in our flow solvers in conjunction with an inexact Newton strategy [11]. The reason for this is most likely accounted for by the fact that $(\nabla_{Q^n} R^{*n})^T$ is more diagonally dominant than the steady flow Jacobian $(\nabla_Q R)^T$ due to the extra terms on the diagonal, which makes this matrix more suited for the use of Bi-CGSTAB. However, for the unsteady flow solvers we still use the GMRES method because there are no significant computational savings for the few linear iterations we use per nonlinear (outer) iteration.

We also found that the algebraic grid movement algorithm used by Nemeč and Zingg [25] is not capable of dealing with the occasional fairly large shape changes. Thus we use a linear elasticity mesh movement method [26] with three increments.

4 RESULTS

The laminar flow around the original Blake airfoil exhibits unsteady vortex shedding, which leads to an oscillatory cost function as shown in Figure 2 using a time step size of $\Delta t = 0.005$. The agreement between our cost function for the original Blake airfoil and the one shown in Marsden *et al.* [8] is very good, even though our grid is about five times coarser.

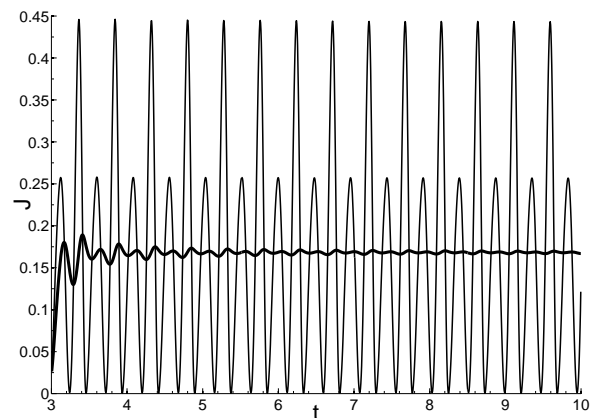


Figure 2: Instantaneous (thin line) and time-averaged (thick line) cost function for the original Blake airfoil vs. time ($\Delta t = 0.005$).

In the actual optimization runs we use the discrete version of the time-averaged cost function given by equation (9) once it is sufficiently converged. After each shape modification the flow solve is warmstarted from the original Blake airfoil periodic steady state solution and the flow is allowed to evolve for some time

to establish a new periodic steady state before the cost function is calculated (see Figure 6). We “jump” over this unphysical adjusting period as quickly as possible by taking a bigger time step $\Delta T = 0.01$ for the first $N^* = 300$ steps. Once we reach our desired control window (where we time average the objective function), we use a smaller time step $\Delta t = 0.005$ for another 1400 steps, for a total of $N = 1700$ time steps covering a time interval of $[0, 10]$ for each flow solve. The corresponding adjoint equations for this situation are given in Rumpfkeil and Zingg [9].

We start the optimization procedure from four different initial shapes, which are shown together with their objective function values (without the quadratic penalty for thickness constraint violation) in Figure 3:

1. The original Blake airfoil (in red)
2. The airfoil defined through the thickness constraint line (in green)
3. The airfoil that results from setting all twelve design variables to their specified upper bound (in blue)
4. The airfoil that results from setting all twelve design variables to their specified lower bound (in black)

The first three initial shapes do not violate any thickness constraints; however, the fourth one does.

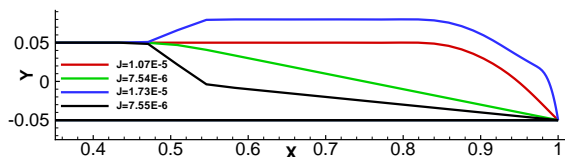


Figure 3: The initial airfoil shapes.

The convergence histories of these aeroacoustic shape design problems are shown in Figure 4. The objective functions are always scaled with the initial objective function value of the original Blake airfoil $J_0 = 1.07 \cdot 10^{-5}$ to ease comparisons.

One can see that all objective functions are driven to much smaller values in about four to six design iterations and that the improvement after that is only marginal. Starting from the original Blake airfoil leads to the best airfoil in terms of total radiated acoustic power. The reduction is about 95 percent from the initial value and thus much larger than the 80 percent achieved by Marsden *et al.* [8] using five design variables.

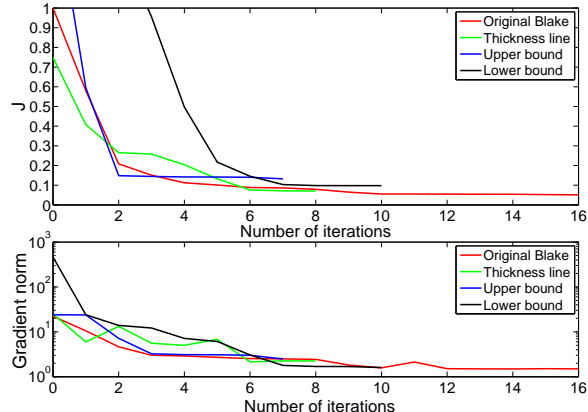


Figure 4: Convergence histories of the aeroacoustic shape design problems using twelve design variables.

The gradient norms are only reduced by one to two orders of magnitude, implying that the optimizer did not converge to an optimum. The reason for this is that we specified lower and upper bounds for the design variables to prevent grid perturbations that are too large which result in convergence problems for the linear elasticity mesh movement solver. Some of the design variables are at their upper bound as can be seen in Figure 5 and the optimizer would like to increase their values even further, thus it is not possible for the optimizer to reach the optimum.

Figure 5 shows the final optimized airfoil shapes, which are very interesting and completely unexpected. The increase in the trailing-edge angle to decrease the trailing-edge noise was also found by Marsden *et al.* and was theoretically predicted by Howe [27] for turbulent flow. However, the “wavy” part of the airfoil is a novel result and to the best of the authors’ knowledge has not been reported by other researchers. Presumably Marsden *et al.* did not obtain similar “wavy” shapes due to the fact that they used only five design variables and thus did not give their optimizer enough freedom to come up with these novel shapes.

	Initial			Optimized		
	\bar{C}_L	\bar{C}_D	$\frac{\bar{C}_L}{\bar{C}_D}$	\bar{C}_L	\bar{C}_D	$\frac{\bar{C}_L}{\bar{C}_D}$
Original Blake	0.272	0.074	3.68	0.272	0.049	5.55
Thickness line	0.248	0.054	4.59	0.264	0.050	5.28
Upper bound	0.222	0.097	2.29	0.280	0.061	4.59
Lower bound	0.240	0.059	4.07	0.284	0.057	4.98

Table 1: A comparison of the mean lift and drag coefficients for the initial and optimized airfoils.

A comparison of the mean lift and drag coefficients for the initial and optimized airfoils is displayed in Table 1. We do not have to add a lift constraint or a penalty for decreased lift to the objective function

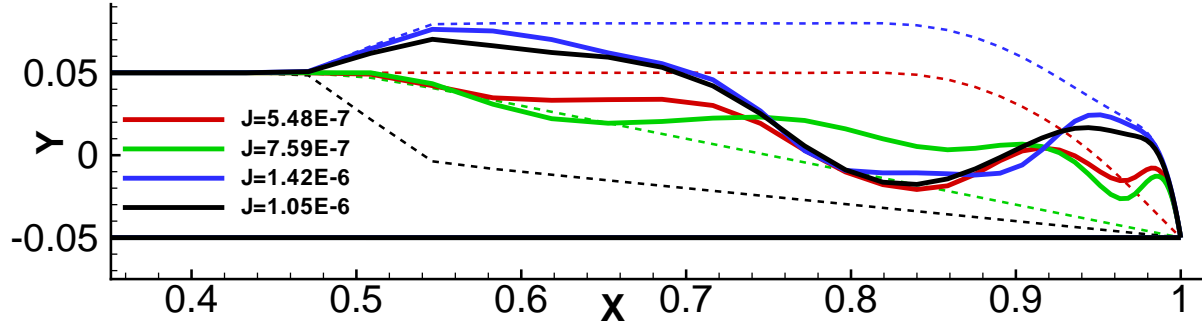


Figure 5: Final optimized airfoil shapes.

since the mean lift coefficients for all optimized airfoils either stay the same or increase in comparison to their initial values. This means the optimizer has not only produced aeroacoustically improved airfoils, but also as a byproduct the initial airfoils have been aerodynamically enhanced.

The time histories of C_L and C_D for the original Blake airfoil before and after the optimization are shown in Figure 6. One can clearly see the unphysical adjusting period for the optimized airfoil in the time interval $[0, 3]$ before it reaches its new periodic steady state. A reduced mean drag as well as reduced oscillation amplitudes for the optimized airfoil are also visible.

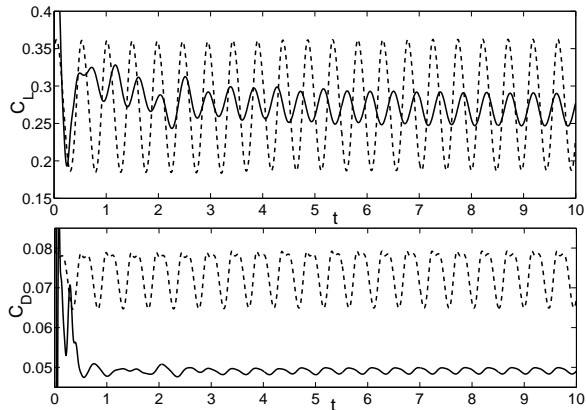


Figure 6: Time histories of C_L and C_D for the original Blake airfoil. The histories of the initial (dotted) and optimized (solid) airfoils vs. time ($\Delta t = 0.005$) are shown.

We also tried to save computational time and storage by saving the flowfield in the control window only every second time step. We have used this approach very successfully in previous studies [9, 28]. However, in this case this approach does not work very well since the optimizer is barely able to improve the initial airfoils even slightly with this inexact gradient information.

5 CONCLUSION

The discrete adjoint method was successfully applied to unsteady laminar trailing edge optimization resulting in a significant reduction in the total radiated acoustic power. The resulting optimized airfoils showcase very interesting and completely unexpected shapes, thereby showing the power of numerical shape optimization, which can lead to counter-intuitive results. The general framework presented to derive the unsteady discrete adjoint equations for optimal control can also be used for many other inherently unsteady optimization problems. Our future work will focus on the ability to modify a high-lift airfoil configuration to reduce the radiated noise while maintaining good performance.

ACKNOWLEDGMENTS

The funding of the second author by the Natural Sciences and Engineering Research Council of Canada and the Canada Research Chairs program is gratefully acknowledged.

REFERENCES

- [1] S. Obayashi. *Aerodynamic Optimization with Evolutionary Algorithms*. Inverse Design and Optimization Methods, Lecture Series 1997-05, edited by R. A. V. den Braembussche and M. Manna, Von Karman Institute for Fluid Dynamics, Brussels, 1997.
- [2] A. Jameson, N.A. Pierce, and L. Martinelli. Optimum Aerodynamic Design Using the Navier-Stokes Equations. *Theoretical and Computational Fluid Dynamics*, Vol. 10, No. 1:pp. 213–237, 1998.
- [3] W. K. Anderson and D. L. Bonhaus. Airfoil Design on Unstructured Grids for Turbulent Flows. *AIAA Journal*, Vol. 37, No. 2:pp. 185–191, 1999.

- [4] M. Nemeć and D.W. Zingg. Newton-Krylov Algorithm for Aerodynamic Design Using the Navier-Stokes Equations. *AIAA Journal*, Vol. 40, No. 6:pp. 1146–1154, 2002.
- [5] B.A. Singer, K.S. Brentner, and D.P. Lockard. Computational Aeroacoustic Analysis of Slat Trailing-Edge Flow. *AIAA Journal*, Vol. 38, No. 9:pp. 1558–1564, 2000.
- [6] M.R. Khorrami, M.E. Berkman, and M. Choudhari. Unsteady Flow Computations of a Slat with a Blunt Trailing Edge. *AIAA Journal*, Vol. 38, No. 11:pp. 2050–2058, 2000.
- [7] B.A. Singer and Y. Guo. Development of Computational Aeroacoustics Tools for Airframe Noise Calculations. *International Journal of Computational Fluid Dynamics*, Vol. 18(6):pp. 455–469, 2004.
- [8] A.L. Marsden, M. Wang, J.E. Dennis Jr., and P. Moin. Optimal Aeroacoustic Shape Design Using the Surrogate Management Framework. *Optimization and Engineering*, Vol. 5(2):pp. 235–262, 2004.
- [9] M. Rumpfkeil and D.W. Zingg. A General Framework for the Optimal Control of Unsteady Flows with Applications. AIAA, 2007-1128, 2007.
- [10] S. Isono and D.W. Zingg. A Runge-Kutta-Newton-Krylov Algorithm for Fourth-Order Implicit Time Marching Applied to Unsteady Flows. AIAA, 2004-0433, 2004.
- [11] A. Pueyo and D.W. Zingg. Efficient Newton-Krylov Solver for Aerodynamic Computations. *AIAA Journal*, Vol. 36, No. 11:pp. 1991–1997, 1998.
- [12] C.G. Broyden. The Convergence of a Class of Double-Rank Minimization Algorithms. *Journal Inst. Math. Applic.*, Vol. 6:pp. 76–90, 1970.
- [13] R. Fletcher. A New Approach to Variable Metric Algorithms. *Computer Journal*, 13:pp. 317–322, 1970.
- [14] D. Goldfarb. A Family of Variable Metric Updates Derived by Variational Means. *Mathematics of Computing*, Vol. 24:pp. 23–26, 1970.
- [15] D.F. Shanno. Conditioning of Quasi-Newton Methods for Function Minimization. *Mathematics of Computing*, Vol. 24:pp. 647–656, 1970.
- [16] W.K. Blake. A statistical description of pressure and velocity fields at the trailing edge of a flat strut. DTNSRDC Report 4241, David Taylor Naval Ship R & D Center, Bethesda, Maryland, 1975.
- [17] N. Curle. The influence of solid boundary upon aerodynamic sound. *Proc. Royal Soc. Lond. A*, 231:505-514, 1955.
- [18] A.L. Marsden, M. Wang, and P. Koumoutsakos. Optimal aeroacoustic shape design using approximation modeling. Annual Research Briefs, Center for Turbulence Research, Stanford University, 2002.
- [19] M. Wang, S.K. Lele, and P. Moin. Computation of quadrupole noise using acoustic analogy. *AIAA Journal*, Vol. 34, No. 11:pp. 2247–2254, 1996.
- [20] R. H. Byrd, P. Lu, J. Nocedal, and C. Zhu. A Limited Memory Algorithm for Bound Constrained Optimization. *SIAM J. Scientific Computing* 16, Vol. 5:pp. 1190–1208, 1995.
- [21] C. Zhu, R.H. Byrd, P. Lu, and J. Nocedal. L-BFGS-B: A Limited Memory FORTRAN Code for Solving Bound Constrained Optimization Problems. Technical Report NAM-11, EECS Department, Northwestern University, 1994.
- [22] T. H. Pulliam. *Efficient Solution Methods for the Navier-Stokes Equations*. Lecture Notes for the Von Karman Institute For Fluid Dynamics Lecture Series, 1986.
- [23] H. van der Vorst. Bi-CGSTAB: A Fast and Smoothly Converging Variant of Bi-CG for the Solution of Nonsymmetric Linear Systems. *SIAM Journal on Scientific and Statistical Computing*, Vol. 13:631–644, 1992.
- [24] Y. Saad and M.H. Schultz. GMRES: A Generalized Minimal Residual Algorithm for Solving Nonsymmetric Linear Systems. *SIAM Journal on Scientific and Statistical Computing*, Vol. 7 No. 3:856–869, 1986.
- [25] M. Nemeć and D.W. Zingg. Multipoint and Multi-Objective Aerodynamic Shape Optimization. *AIAA Journal*, Vol. 42, No. 6:pp. 1057–1065, 2004.
- [26] A.H. Truong, C. Oldfield, and D.W. Zingg. A Linear Elasticity Mesh Movement Method with an Augmented Adjoint Approach for Aerodynamic Shape Optimization. Proceedings of the

12th Annual CASI Aerodynamics Symposium,
Toronto, paper 317, 2007.

- [27] M.S. Howe. The influence of surface rounding on trailing edge noise. *Journal of Sound and Vibration*, Vol. 126, No. 3:pp. 503–523, 1988.
- [28] M. Rumpfkeil and D.W. Zingg. The Remote Inverse Shape Design of Airfoils in Unsteady Flows. Proceedings of the 12th Annual CASI Aerodynamics Symposium, Toronto, paper 318, 2007.